INFORMATICS JOURNALS

Research Article

Journal of Natural Remedies
DOI: 10.18311/jnr/2026/54030

eISSN: 2320-3358 | Vol 26(3), 2026 | pp. 723-739

Formulation and Characterisation of Hyaluronic Acid-coated Chitosan Nanoparticles Loaded with Thymoquinone for Targeted Therapy in Rheumatoid Arthritis

Madhavi Patel[1], M. K. Mohan Maruga Raja[2] and Ravi Manne[3*]

[1]Department of Pharmacognosy, Parul Institute of Pharmacy, Faculty of Pharmacy, Parul University, Waghodia, Vadodara – 391760, Gujarat, India

[2]East Point College of Pharmacy, Bengaluru – 560049, Karnataka, India

[3]Faculty of Pharmacy, Parul University, Waghodia, Vadodara – 391760, Gujarat, India; ravimanne66@gmail.com

Abstract

Background: Rheumatoid arthritis (RA) is a chronic autoimmune disorder that causes persistent joint inflammation and progressive structural damage, leading to significant disability. Conventional treatments such as DMARDs and biologics improve outcomes but remain constrained by toxicity, immunosuppression, and high cost, creating the need for safer, more efficient strategies. **Aim:** In this study, thymoquinone (TQ) was encapsulated in hyaluronic acid (HA)–chitosan (Ch) nanoparticles to improve therapeutic delivery. **Methods:** A Central Composite Design (CCD) was employed to systematically evaluate the effects of HA and Ch concentrations on particle size, polydispersity index (PDI), entrapment efficiency (EE), and drug release. **Results:** The nanoparticles produced ranged from 121.6–289.4 nm in size, with PDI values of 0.217–0.667, EE between 89.74–98.74%, and cumulative release of 83.67–90% at 49h. The optimised formulation (HA 0.25 mg/mL, Ch 0.75 mg/mL) yielded particles of ~208 nm, PDI 0.387, EE ~98.7%, sustained release of ~86.6%, and a zeta potential of –28.7 mV. FTIR confirmed drug–polymer compatibility, TEM images revealed spherical morphology, and statistical modelling validated robust optimisation. **Conclusion:** These results establish F6 Ch nanoparticles as a reproducible platform with favourable stability, encapsulation, and controlled release, offering strong potential for targeted RA therapy.

Major Findings: Hyaluronic acid–chitosan nanoparticles were successfully optimised for thymoquinone delivery, achieving nanoscale size, uniform distribution, high drug entrapment, and stable surface charge. The formulation exhibited sustained drug release and improved thymoquinone dispersion, enhancing its potential bioavailability. The optimized formulation showed a nanoscale size (~208 nm), good uniformity, high drug entrapment (~98.7%), and a stable negative surface charge. Overall, the system shows strong promise as a controlled delivery platform for rheumatoid arthritis treatment.

Keywords: Central Composite Design, Controlled Release, Drug Delivery, Hyaluronic Acid–chitosan Nanoparticles, Rheumatoid Arthritis, Thymoquinone

(Article Chronicle: Article Received on: 12.12.2025; Revised on: 17.02.2026; Accepted on: 03.03.2026)

1. Introduction

Rheumatoid arthritis (RA) is a chronic autoimmune disease that progressively damages joints through sustained synovial inflammation, pannus development, and degradation of cartilage and bone. These pathological events ultimately cause deformities, functional impairment, and poor quality of life. The global burden of RA remains considerable, with over 17 million people affected as of 2020, and projections indicating a continued rise in prevalence[1,2]. Women are disproportionately affected, partly due to hormonal and biological influences on immune function.

*Author for correspondence

Current therapy is centred around disease-modifying antirheumatic drugs (DMARDs), corticosteroids, and biologic agents. While these approaches have improved patient outcomes, their clinical use is limited by systemic toxicity, immunosuppression, variable therapeutic response, and economic barriers[3,4]. This underscores the need for safer and more accessible treatment options.

Natural compounds are increasingly explored as adjuncts or alternatives in RA because of their multitarget activity. Thymoquinone (TQ), the major bioactive molecule from *Nigella sativa*, has shown strong anti-inflammatory and antioxidant potential by suppressing nuclear factor-κB (NF-κB) activation and reducing pro-inflammatory mediators such as TNF-α, IL-1β, and IL-6[5-7]. Its immunomodulatory activity makes it particularly relevant for autoimmune disorders, including RA. However, TQ is constrained by poor aqueous solubility, instability under physiological conditions, a short half-life, and low oral bioavailability[8,9].

Nanotechnology offers promising solutions to these pharmacokinetic and formulation challenges. Nanoscale carriers improve solubility, prolong circulation, enable controlled release, and take advantage of the enhanced permeability and retention (EPR) effect to accumulate at inflamed sites[10,11]. Chitosan is a widely studied nanocarrier owing to its biocompatibility, mucoadhesion, biodegradability, and ability to open epithelial tight junctions to enhance absorption[12]. Surface functionalization with HA provides additional biological specificity, as HA binds strongly to CD44 receptors overexpressed in inflamed synovial tissues[13]. This modification not only stabilises nanoparticles but also supports targeted delivery to arthritic joints.

Several formulations of TQ, including micelles, lipid-based carriers, and polymeric nanoparticles, have been evaluated with encouraging results[14,15]. However, many previous systems were developed using trial-and-error methods, which compromise reproducibility and translation. To address this, the present work focused on the rational design and systematic optimisation of HA-coated chitosan nanoparticles encapsulating TQ. Particular attention was given to formulation variables influencing particle size, PDI, zeta potential, encapsulation efficiency, and release behaviour. The optimised nanocarrier was then subjected to comprehensive physicochemical and morphological characterisation, stability testing, and release profiling to establish a reproducible platform for potential application in RA therapy.

2. Materials and Methods

2.1 Materials

Thymoquinone (TQ, purity ≥98%) was purchased from Sigma-Aldrich (St. Louis, MO, USA). Chitosan of medium molecular weight (degree of deacetylation ~85%) was procured from HiMedia Laboratories Private Limited (Mumbai, India). Hyaluronic acid (sodium salt, MW 200–400 kDa) and dialysis membranes (MWCO 12–14 kDa) were obtained from Sigma-Aldrich (USA). Sodium tripolyphosphate (TPP, analytical grade), glacial acetic acid, and ethanol (absolute, ≥99.9%) were supplied by Merck (Darmstadt, Germany). Analytical grade phosphate-buffered saline (PBS, pH 7.4) was prepared using NaCl, KCl, Na_2HPO_4, and KH_2PO_4 (HiMedia, India). Tween 80 (Polysorbate 80) was also obtained from Merck. Deionised water was prepared using a Milli-Q system (Millipore, Bedford, MA, USA).

2.2 Screening of Formulation and Process Variables Using Taguchi Design

Critical formulation and process parameters were first screened using the Taguchi design approach, a robust statistical tool that reduces experimental runs while identifying the relative contribution of each factor[16,17]. Based on preliminary studies, four variables were selected: Chitosan concentration (A), TPP concentration (B), Rate of TPP addition (C) and Hyaluronic acid concentration (D).

Table 1. Independent factors and their levels used in the Taguchi design

Factors	Levels		
	1	2	3
A = Concentration of Chitosan (Ch)	0.5 mg/mL	1 mg/mL	1.5 mg/mL
B = Concentration of TPP	0.25 mg/mL	0.75 mg/mL	1.5 mg/mL
C = Rate of addition of TPP	1 mL/min	2 mL/min	3 mL/min
D = Concentration of Hyaluronic acid (HA)	0.2 mg/mL	0.3 mg/mL	0.4 mg/mL

Table 2. Experimental design and independent factors for 9 Taguchi design batches

Experimental No.	Experimental Conditions							
	Variables and levels in coded form				Variables and levels in actual form			
	A	B	C	D	A	B	C	D
1	1	1	1	1	0.5 mg/mL	0.25 mg/mL	1 mL/min	0.2 mg/mL
2	1	2	2	2	0.5 mg/mL	0.75 mg/mL	2 mL/min	0.3 mg/mL
3	1	3	3	3	0.5 mg/mL	1.5 mg/mL	3 mL/min	0.4 mg/mL
4	2	1	2	3	1 mg/mL	0.25 mg/mL	2 mL/min	0.4 mg/mL
5	2	2	3	1	1 mg/mL	0.75 mg/mL	3 mL/min	0.2 mg/mL
6	2	3	1	2	1 mg/mL	1.5 mg/mL	1 mL/min	0.3 mg/mL
7	3	1	3	2	1.5 mg/mL	0.25 mg/mL	3 mL/min	0.3 mg/mL
8	3	2	1	3	1.5 mg/mL	0.75 mg/mL	1 mL/min	0.4 mg/mL
9	3	3	2	1	1.5 mg/mL	1.5 mg/mL	2 mL/min	0.2 mg/mL

Each variable was studied at three levels, and an L9 (3^4) orthogonal array was applied, generating nine experimental batches (Tables 1 and 2). The primary responses were particle size and polydispersity index (PDI), as both strongly influence nanoparticle stability, biodistribution, and retention at inflamed joints[18-20].

Particle size and polydispersity index (PDI) were selected as primary response variables, as they strongly influence biodistribution, cellular uptake, and retention in inflamed joints. Nanoparticles <200 nm exhibit enhanced permeability and retention (EPR) effect, whereas a PDI <0.3 reflects monodisperse and stable formulations[19,20].

Dynamic light scattering (DLS) using a Malvern Nano Zetasizer (Nano-S90) was employed to measure particle size and PDI. The Taguchi model incorporated signal-to-noise (S/N) ratio analysis with the "smaller-the-better" criterion, since smaller particle size and lower PDI are desirable. Main effects, delta values, and factor ranking were analysed to determine the most influential variables and their optimised levels[21,22].

2.3 Formulation Optimisation

Following the Taguchi analysis, further optimisation of the nanoparticle formulation was performed using a face-centred Central Composite Design (CCD) to comprehensively evaluate the effect of formulation variables and their interactions on critical quality attributes (CQAs). CCD is widely recognised in pharmaceutical research for providing a robust quadratic model that allows prediction of both linear and non-linear effects with reduced experimental runs, while ensuring statistical reliability[23,24].

In this study, two independent factors were selected: the concentration of Hyaluronic acid (HA) and Chitosan (Ch), each at three levels, as summarised in Tables 3 and 4. The dependent responses optimised were particle size, polydispersity index (PDI), entrapment efficiency (EE), and drug release profile, as these parameters critically determine nanoparticle stability, bioavailability, and therapeutic efficiency[25-27].

The selected design allowed evaluation of main effects, interactive effects, and quadratic influence of the polymeric concentrations on the critical quality attributes. The model adequacy was further verified by statistical analysis (ANOVA), ensuring the predictive reliability of the fitted quadratic equations.

2.4 Preparation of Nanoparticles

HA-coated TQ-loaded chitosan nanoparticles were fabricated by ionic gelation[28–30]. Chitosan (0.5–1.0 mg/mL) was dissolved in 1% v/v acetic acid and left overnight for complete hydration. TQ (1% w/v), dissolved in a small volume of ethanol, was added dropwise to the chitosan solution under stirring. The pH of the dispersion was adjusted to 4.5 using 0.2 M NaOH to favour electrostatic interactions between protonated chitosan and anionic TPP. A freshly prepared TPP solution (0.25 mg/mL) was then introduced at a controlled rate (1 mL/min) with continuous stirring for 30 min, promoting nanoparticle assembly via ionic crosslinking. Subsequently, HA solution (0.2–0.3 mg/mL) was added dropwise under

stirring, enabling HA adsorption onto the nanoparticle surface through electrostatic and hydrogen bonding interactions. The resulting HA–Ch nanoparticles were stored at 4 °C until further analysis[31–34].

3. Characterisation

3.1 Particle Size and Polydispersity Index (PDI)

Dynamic light scattering (DLS) was carried out using a Malvern Zetasizer Nano-S90 (Malvern Instruments, UK). Samples were diluted with deionised water before measurement to avoid multiple scattering effects[28].

3.2 Entrapment Efficiency (EE)

Two millilitres of nanoparticle suspension were centrifuged at 13,000 rpm for 2 h at 4 °C (Remi Cooling Centrifuge, India). The supernatant was diluted with PBS (pH 7.4), and the concentration of free TQ was determined at 257 nm using a UV–visible spectrophotometer (UV-1800, Shimadzu, Japan). Entrapment efficiency was calculated as: EE was calculated using the following equation[29]:

$$Entrapment\ ef\ ficiency = \frac{Total\ drug - Free\ drug}{Total\ drug} \times 100$$

3.3 *In Vitro* Drug Release

The release study was conducted using a Franz diffusion cell (diffusion area 2.5 cm^2). Five mL of nanoparticle suspension was placed in the donor compartment, separated from the receptor medium (25 mL PBS, pH 7.4) by a pre-hydrated dialysis membrane. The receptor phase was maintained at 37 ± 0.5 °C with constant stirring (100 rpm). Samples were withdrawn at predetermined intervals and replaced with fresh buffer. The released TQ was quantified at 257 nm[30].

Table 3. Independent factors and their levels used in CCD

Factors	Levels		
	-1	0	+1
A = Concentration of Hyaluronic acid (HA) (mg/mL)	0.2	0.25	0.3
B = Concentration of Chitosan (Ch) (mg/mL)	0.5	0.75	1

3.4 Differential Scanning Calorimetry (DSC)

Thermal properties were examined using a DSC-60 Plus (Shimadzu, Japan). Samples of pure drug, polymers, physical mixtures, and nanoparticles were sealed in aluminium pans and heated from 25 to 300 °C at 10 °C/min under nitrogen (50 mL/min)[31].

3.5 Fourier Transform Infrared Spectroscopy (FTIR)

FTIR spectra were recorded using an ATR-FTIR spectrometer (Bruker Alpha II, Germany). Measurements were carried out in the 400–4000 cm^{-1} range at 4 cm^{-1} resolution to evaluate possible interactions between the drug and polymers[32].

3.6 Transmission Electron Microscopy (TEM)

Morphological examination was performed using TEM (JEOL JEM-2100, Japan). A drop of nanoparticle dispersion was placed on carbon-coated copper grids, negatively stained with 1% phosphotungstic acid, and air-dried before imaging at an accelerating voltage of 200 kV[33,34].

4. Results and Discussion

4.1 Screening of Formulation and Process Parameters

Preliminary screening was conducted to evaluate the influence of formulation and process parameters—including chitosan concentration, TPP concentration,

Table 4. Experimental design and independent factors for face-centred CCD

Experimental No.	Experimental Conditions			
	Variables and levels in coded form		Variables and levels in actual form	
	A	B	A	B
1	0	0	0.25	0.75
2	-1	1	0.2	1
3	0	-1	0.25	0.5
	-1	0	0.2	0.75
	0	1	0.25	1
	1	1	0.3	1
	1	-1	0.3	0.5
	1	0	0.3	0.75
	-1	-1	0.2	0.5

A= Concentration of Hyaluronic acid (HA) (mg/mL); B= Concentration of Chitosan (Ch) (mg/mL)

HA concentration, acetic acid percentage, stirring speed, and rate of TPP addition—on particle size and polydispersity index (PDI). The study revealed that chitosan concentration, TPP concentration, HA concentration, and TPP addition rate were the most critical determinants of nanoparticle characteristics (Tables 1 and 2). In contrast, acetic acid concentration (1–6%) and stirring speed (up to 500 rpm) exhibited negligible effects on particle size and PDI, and were therefore fixed in subsequent optimisation studies[35,36].

At low-to-moderate chitosan concentrations (0.5–1.0 mg/mL), nanoparticles with smaller diameters (<200 nm) and narrow size distributions (PDI <0.3) were obtained, reflecting reduced polymer entanglement and enhanced chain flexibility. However, at higher concentrations (>1.0 mg/mL), particle size (>300 nm) and PDI (>0.5) increased significantly due to elevated viscosity and polymer crowding that hindered efficient nucleation[37]. Similarly, an optimal TPP concentration of 0.5–0.75 mg/mL was identified; insufficient TPP caused incomplete crosslinking, while excessive concentrations (>1.5 mg/mL) induced over-crosslinking, leading to aggregation and heterogeneity[38]. The TPP addition rate also proved critical: slow addition (1 mL/min) facilitated uniform ionic gelation and produced smaller nanoparticles (<200 nm), whereas rapid addition (≥2 mL/min) disrupted controlled assembly, resulting in larger, polydisperse particles[39]. HA concentration between 0.2 and 0.3 mg/mL provided stable surface coating and steric stabilisation, yielding monodisperse nanoparticles. In contrast, excessive HA (>0.3 mg/mL) triggered bridging flocculation and instability, as reflected by PDI values approaching unity[40,41].

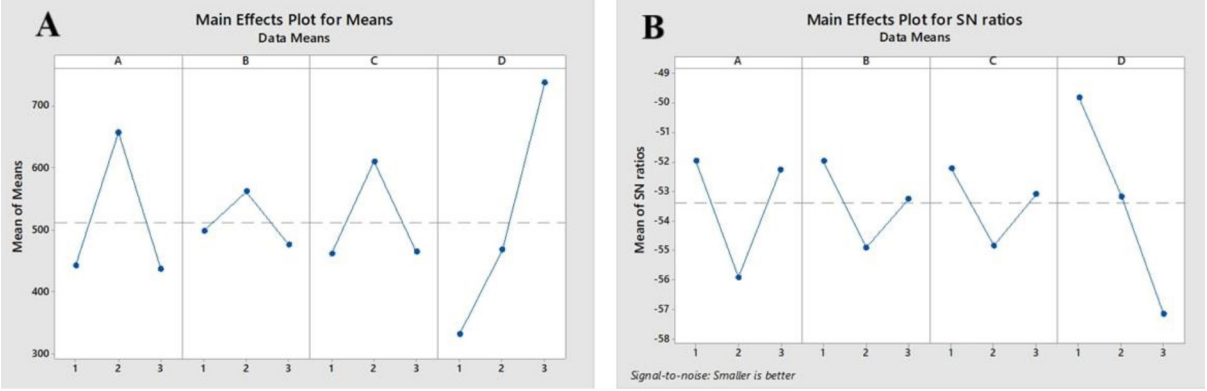


Figure 1. Factor response graph of particle size; **(A).** Main Effects Plot for Means, **(B).** Main Effects Plot for SN ratios.

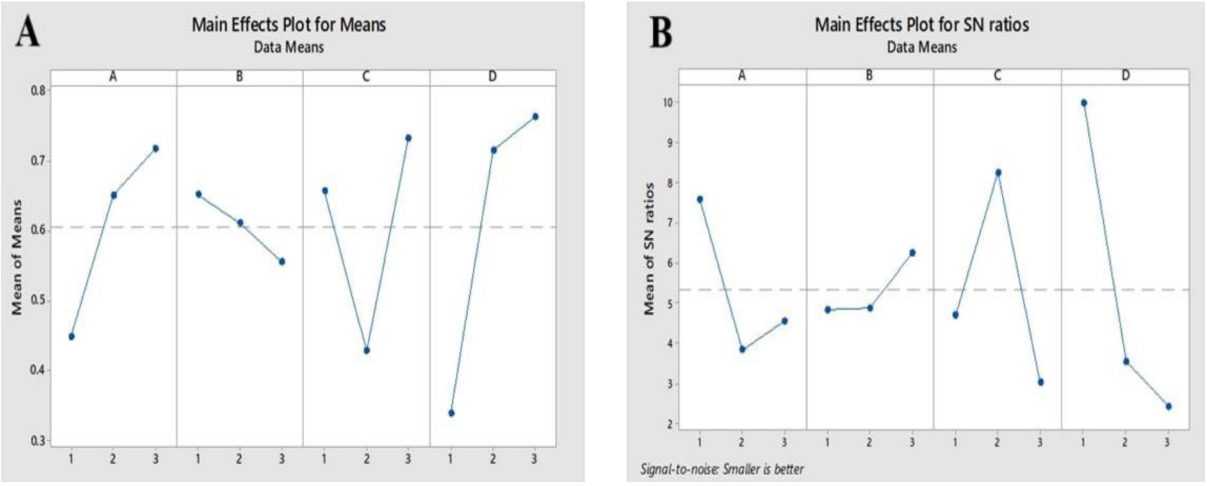


Figure 2. Factor response graph of PDI; **(A).** Main Effects Plot for Means, **(B).** Main Effects Plot for SN ratios.

4.2 Taguchi Design and ANOVA Analysis

A Taguchi L9 orthogonal array was implemented to systematically examine the four critical factors—chitosan concentration (A), TPP concentration (B), TPP addition rate (C), and HA concentration (D)—on particle size and PDI. Signal-to-noise (S/N) ratio plots using the "smaller-the-better" criterion indicated that all variables significantly influenced both particle size and PDI, with HA concentration emerging as the most dominant contributor, followed by chitosan concentration and TPP addition rate (Figures 1 and 2, Table 4). One-way ANOVA confirmed these findings, demonstrating statistically significant effects ($p < 0.05$) for all parameters across both responses.

For particle size, HA concentration exhibited the highest F-ratio, underscoring its pivotal role in governing nanoparticle dimensions, consistent with previous reports that surface-coating polymers critically determine nanoparticle stability and final size[40,42]. Regarding PDI, HA concentration and TPP addition rate were particularly influential, as rapid TPP addition and excessive HA led to broad size distributions and colloidal instability. Conversely, optimised conditions comprising low-to-moderate chitosan (0.5–1.0 mg/mL), moderate TPP (0.5–0.75 mg/mL), slow TPP addition (1 mL/min), and HA within 0.2–0.3 mg/mL consistently yielded nanoparticles <200 nm with PDI <0.3, confirming robust control over size and dispersity.

These findings highlight that precise regulation of polymer and crosslinker concentrations, together with controlled gelation kinetics, is essential for generating stable, monodisperse HA-coated chitosan nanoparticles. The Taguchi design approach thus provided a reliable statistical framework to identify key variables and establish optimal fabrication conditions, ensuring reproducibility and scalability in nanoparticle production for targeted rheumatoid arthritis therapy[35-43].

4.3 Preparation of Nanoparticles

The successful fabrication of thymoquinone-loaded chitosan nanoparticles was confirmed through the ionic gelation approach, wherein formulation variables were carefully tuned to achieve stable and reproducible systems. Chitosan, owing to its cationic nature, was first solubilised in dilute acetic acid, yielding a homogeneous polymeric solution with protonated amino groups conducive to crosslinking. The pH adjustment to 4.5 was crucial, as it optimised the ionisation state of chitosan, thereby facilitating controlled interactions with the anionic tripolyphosphate (TPP). The dropwise addition of TPP resulted in instantaneous nanoparticle nucleation via electrostatic interactions, leading to discrete nanosized structures with minimal aggregation. Uniform dispersion of thymoquinone within the chitosan matrix ensured efficient drug loading and prevented crystallisation of the lipophilic drug within the aqueous system. Subsequent hyaluronic acid (HA) coating imparted steric stabilisation, reduced interparticle collisions, and enhanced colloidal stability through hydrophilic shell formation. The HA layer further introduced targeting potential owing to CD44 receptor affinity, a feature particularly advantageous for inflamed synovial tissues in rheumatoid arthritis therapy. Overall, the nanoparticle preparation process demonstrated precise control over ionic gelation and surface modification, yielding a formulation with favourable stability and drug incorporation consistent with prior reports on chitosan–TPP nanosystems[44,45].

4.4 Optimisation of Formulation

A face-centred Central Composite Design (CCD) was employed to investigate the impact of hyaluronic acid (HA, factor A) and chitosan (Ch, factor B) concentrations on particle size, polydispersity index (PDI), entrapment efficiency (EE), and drug release. Nine experimental formulations were generated with coded levels (−1, 0, +1), and their responses are summarised in Table 5. The experimental data demonstrated particle sizes ranging between 121.6 and 289.4 nm, PDI values of 0.217–0.667, EE of 89.74–98.74%, and drug release ranging from 83.67–90%. Statistical significance and interaction effects were analysed using quadratic polynomial models, 3D surface, and contour plots.

4.4.1 Effect on Particle Size

ANOVA confirmed that both HA (A) and chitosan (B) concentrations significantly affected particle size ($p = 0.0002$ and 0.0007, respectively). The quadratic model was:

$$Particlesize = +209.91 - 49.37A - 33.55B + 1.87\ AB + 1.73A2 - 7.62B2$$

The negative coefficients for A (−49.37) and B (−33.55) indicate that increasing either HA or chitosan reduces nanoparticle size, with HA exerting a stronger effect. This was corroborated by response surface plots

as shown in Figure 3 (A and B), where the lowest particle sizes (<150 nm) were obtained at higher polymer concentrations. Mechanistically, increasing HA (anionic) and chitosan (cationic) enhances electrostatic interactions during ionic gelation, leading to denser, more compact particles. Stronger polyelectrolyte complexation reduces polymer chain relaxation, thereby minimising hydrodynamic diameter. Moreover, higher concentrations reduce interfacial tension and favour rapid nucleation over growth, yielding smaller nanoparticles with narrow distributions[46,47].

4.4.2 Effect on Polydispersity Index (PDI)

The ANOVA revealed both HA (p = 0.0011) and chitosan (p = 0.0094) as significant factors for PDI. The quadratic model was:

$$PDI = +0.3903 - 0.1447\,A - 0.0688\,B + 0.0160\,A2 + 0.0245\,B2$$

Negative coefficients for A and B indicate that higher concentrations of either polymer improve homogeneity by lowering PDI values (<0.3). HA displayed a stronger influence, consistent with its surface-coating role in stabilising nanoparticles. Figure 4A and 4B depict the response surface curve. Mechanistically, elevated HA and chitosan concentrations accelerate controlled nucleation and suppress uncontrolled growth, leading to monodisperse systems. The hydrophilic HA coating reduces interparticle collisions and prevents bridging flocculation, while denser chitosan–TPP crosslinking minimises aggregation. Together, these factors promote uniform size distribution[48,49].

4.4.3 Effect on Entrapment Efficiency (EE)

The quadratic model for EE was statistically non-significant (F = 0.8855, p = 0.5789), with poor fit statistics ($R^2 = 0.5961$, Adjusted $R^2 = -0.0771$, Predicted $R^2 = -2.7584$). The model equation was:

$$EF = +96.06 - 0.7650\,A - 0.3850\,B - 0.4175\,AB - 0.6883\,A2 - 4.08\,B2$$

Although mean EE values remained high (89–99%), the lack of statistical significance suggests minimal variability across formulations. This plateau effect likely reflects near-saturation of drug entrapment within the chitosan matrix, as lipophilic thymoquinone interacts strongly with the polymer backbone (Figure 5A and 5B). While both HA and chitosan contribute to efficient encapsulation through electrostatic and hydrophobic interactions, variations within the tested range did not markedly alter entrapment. Instead, unaccounted variables such as TPP concentration and drug–polymer affinity likely played a more dominant role. Thus, although EE was consistently high, the CCD model failed to capture significant predictive relationships[50,51].

4.4.4 Effect on Drug Release

For drug release, ANOVA confirmed model significance (F = 9.89, p = 0.0409), with chitosan concentration (p = 0.0091) being the dominant factor. The quadratic model was:

$$Drug\ release = +86.30 + 1.11\,A + 2.19\,B$$
$$+0.6921\,AB + 0.5565\,A2 - 0.2349\,B2$$

Positive coefficients for both A and B suggest that increasing HA and chitosan enhances cumulative drug

Table 5. Responses of experimental CCD

Formulation	A	B	Y1	Y2	Y3	Y4
1	0.2	0.5	289.4	0.667	91.54	84.7404
2	0.3	0.5	189.6	0.326	92.64	84.5602
3	0.2	1	213.9	0.51	92.12	86.7173
4	0.3	1	121.6	0.217	91.55	90.0038
5	0.2	0.75	264.5	0.525	96.59	85.1072
6	0.3	0.75	160.4	0.291	91.47	88.6023
7	0.25	0.5	232	0.49	91.54	83.6746
8	0.25	1	174.2	0.343	89.74	89.0342
9	0.25	0.75	208.3	0.387	98.74	86.5842

A = Concentration of Hyaluronic acid (HA) (mg/mL); B = Concentration of Chitosan (Ch) (mg/mL); Y1 = Particle size; Y2 = PDI; Y3 = Entrapment efficiency; Y4 = Drug release, n=3

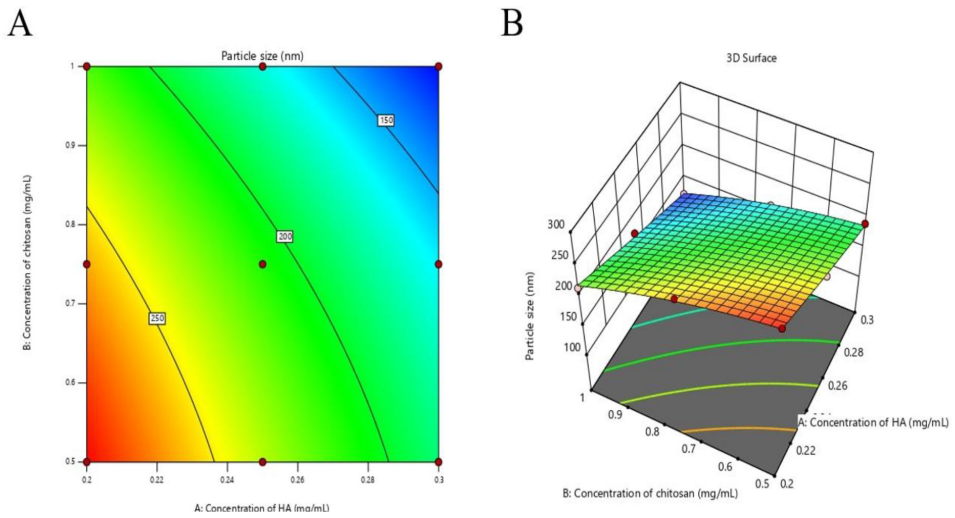


Figure 3. **(A).** Contour plot; **(B).** Response surface graph of Particle size.

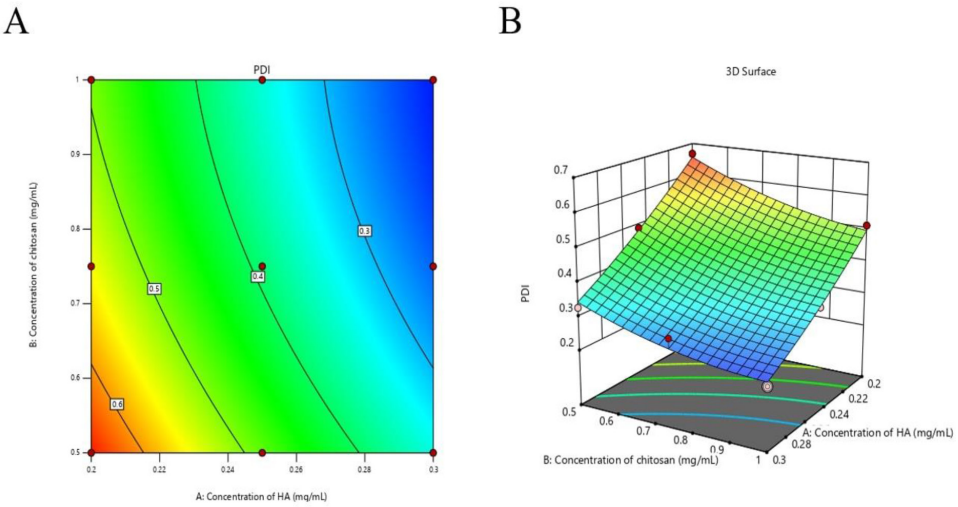


Figure 4. **(A).** Contour plot; **(B).** Response surface graph of PDI.

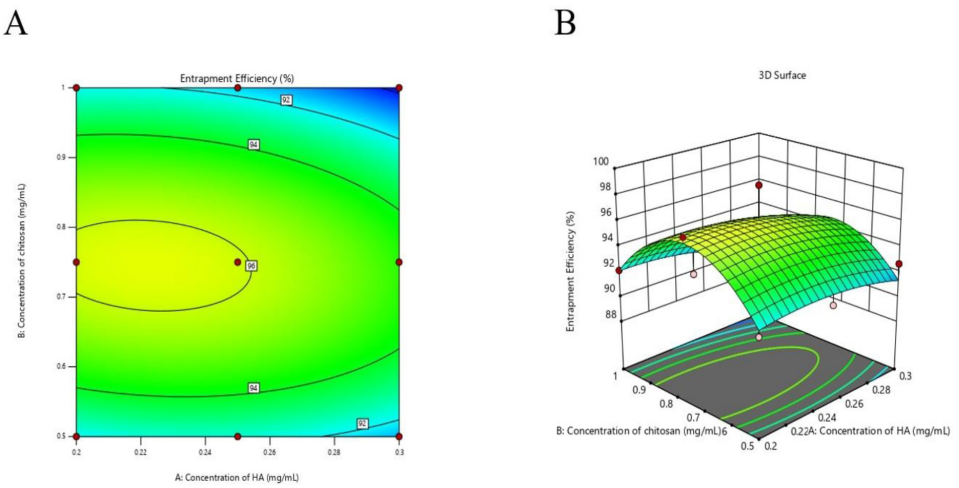


Figure 5. **(A)**. Contour plot; **(B).** Response surface graph of entrapment efficiency.

release. Chitosan exerted a stronger effect (+2.19), likely due to its hydrophilic, porous matrix facilitating drug diffusion (Figure 6A and 6B). HA coating further promoted release by imparting hydration and swelling characteristics that facilitate erosion-assisted diffusion. However, excessive chitosan crosslinking at higher concentrations could potentially slow release, as reflected by the negative quadratic coefficient (−0.2349). Collectively, these findings indicate that moderate-to-high polymer concentrations optimise sustained yet efficient release, consistent with previous reports on polyelectrolyte-based nanoparticle systems[52-54].

4.5 Characterisation of Nanoparticles

4.5.1 Particle Size and PDI

The hydrodynamic size of the nanoparticles ranged from 121.6 to 289.4 nm with a corresponding PDI of 0.217–0.667 as shown in Table 5, signifying nano-dimensionality with variable homogeneity. Increasing concentrations of HA and chitosan produced smaller nanoparticles due to enhanced electrostatic interactions between the anionic HA and cationic amino groups of chitosan, promoting tighter ionic crosslinking and polymer condensation. Higher polymer content reduces interfacial tension, facilitating rapid nucleation and preventing extensive particle growth, thereby favouring smaller sizes. The PDI values indicated that formulations with optimized HA–Ch ratios achieved controlled nucleation and reduced diffusional effects, yielding more uniform particle populations. Conversely, formulations with suboptimal ratios showed higher PDI, likely due to chain entanglement and aggregation effects[55,56].

4.5.2 Entrapment Efficiency (EE)

The formulations exhibited high EE values ranging from 89.74% to 98.74% (Figure 7), which is consistent with the strong ionic interactions between HA and 208 and the hydrophobic partitioning of thymoquinone within the polymeric core. The high surface area-to-volume ratio of nanoparticles further enhances encapsulation. However, ANOVA analysis for EE was statistically non-significant, suggesting limited variability among formulations and possible saturation of polymer binding sites. Once maximum binding is reached, additional polymer concentration exerts minimal influence, producing a plateau effect. Moreover, process variables not included in the CCD model, such as TPP concentration and homogenization dynamics, might have dominated EE outcomes, masking the effect of HA and CS levels. Such high but stable EE values are characteristic of HA-coated CS nanoparticles reported in earlier nanocarrier systems[57,58].

4.5.3 In Vitro Drug Release Study

In vitro release demonstrated a biphasic profile with an initial burst phase followed by sustained release. Among all batches, formulation F4 showed the highest release (~90% at 49 h) as shown in Figure 8. The initial burst can be attributed to surface-adsorbed drug molecules,

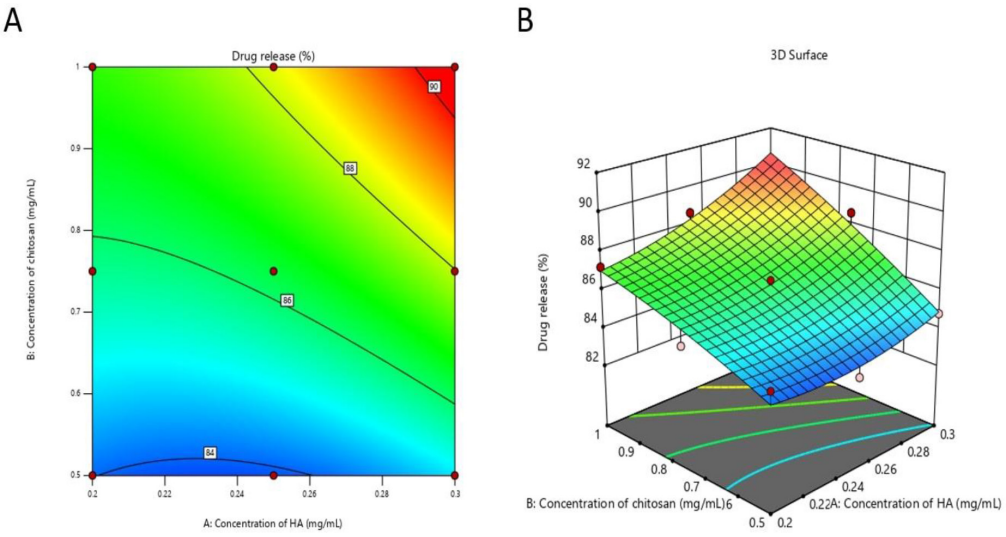


Figure 6. **(A)**. Contour plot; **(B).** response surface graph of drug release.

while the subsequent sustained release is governed by diffusion through the polymer matrix and gradual erosion of HA–Ch complexes. The comparatively higher release in F4 is likely linked to an optimal polymer ratio, which maintained sufficient matrix porosity for diffusion without excessive crosslinking that would hinder release. Such biphasic kinetics are desirable for achieving immediate therapeutic plasma levels followed by extended release, consistent with other HA–Ch nanoformulations designed for controlled delivery[59,60].

Collectively, these findings establish F4, 49j and F8 as the most promising formulations, combining optimal size, homogeneity, high drug loading, and controlled release, and they were subsequently taken forward for further characterisation.

4.5.4 Differential Scanning Calorimetry (DSC)

DSC thermograms revealed significant modifications in thermal behaviour upon nanoparticle formation (Figures 9 and 10). The pure drug displayed a sharp melting endotherm at 48.25 °C, consistent with its crystalline state, whereas this peak disappeared in the nanoparticle formulation, confirming molecular encapsulation and possible amorphisation. Instead, a new endothermic event appeared at ~161 °C in both NP and NP-loaded gel, indicative of drug–polymer interactions or rearrangements within the nanostructure. The broad endothermic transitions observed for HA, chitosan, and Carbopol corresponded to bound and free water evaporation, typical of polysaccharide-based matrices. The persistence of the 161 °C peak in both NP and gel strongly supports stable entrapment within the polymeric network. These results align with earlier reports where encapsulation masked crystalline melting peaks, suggesting enhanced solubility and dissolution potential for poorly soluble drugs[61,62].

4.5.6 Fourier Transform Infrared Spectroscopy (FTIR)

The FTIR spectra in Figures 11 and 12 provide clear evidence of drug–polymer interactions and structural modification following nanoparticle formation. Pure drug exhibited sharp, well-defined peaks corresponding to O–H and C–H stretching (3253–2929 cm^{-1}), carbonyl stretching, and distinct fingerprint vibrations, reflecting its crystalline nature. In contrast, the spectra of drug-loaded nanoparticles (F4, F6, F8) revealed broadening and shifting of the O–H/N–H (~3280–3290 cm^{-1}) and carbonyl (~1650 cm^{-1}) bands, indicating hydrogen bonding and electrostatic interactions between the drug and the chitosan–hyaluronic acid matrix. The disappearance and broadening of sharp peaks confirm disruption of

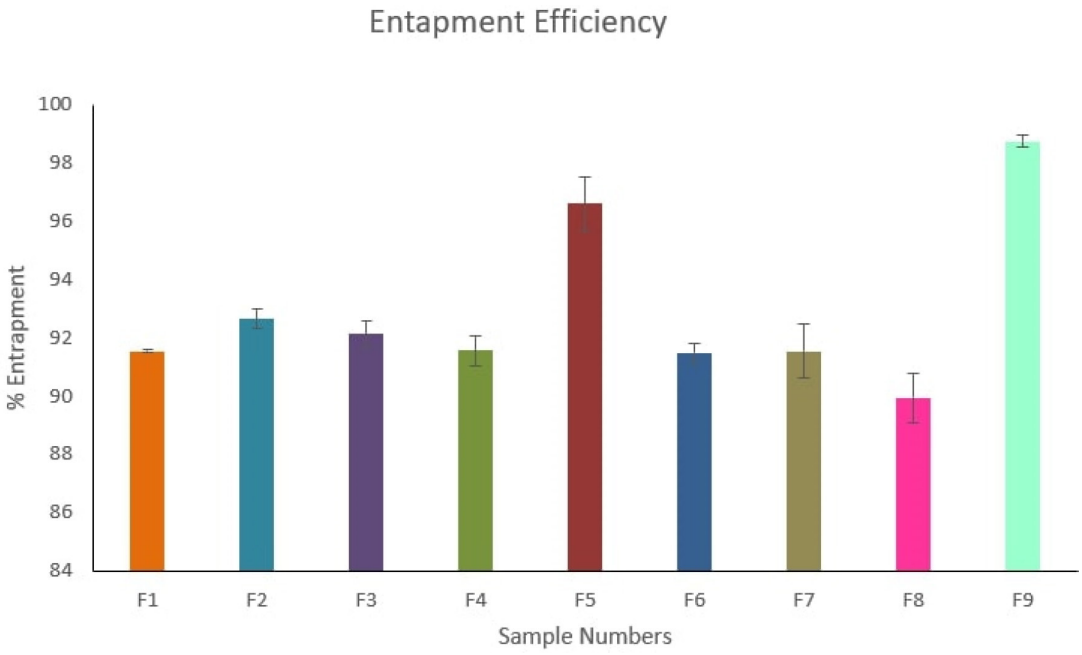


Figure 7. Graphical representation of the entrapment efficiency of all the formulation runs.

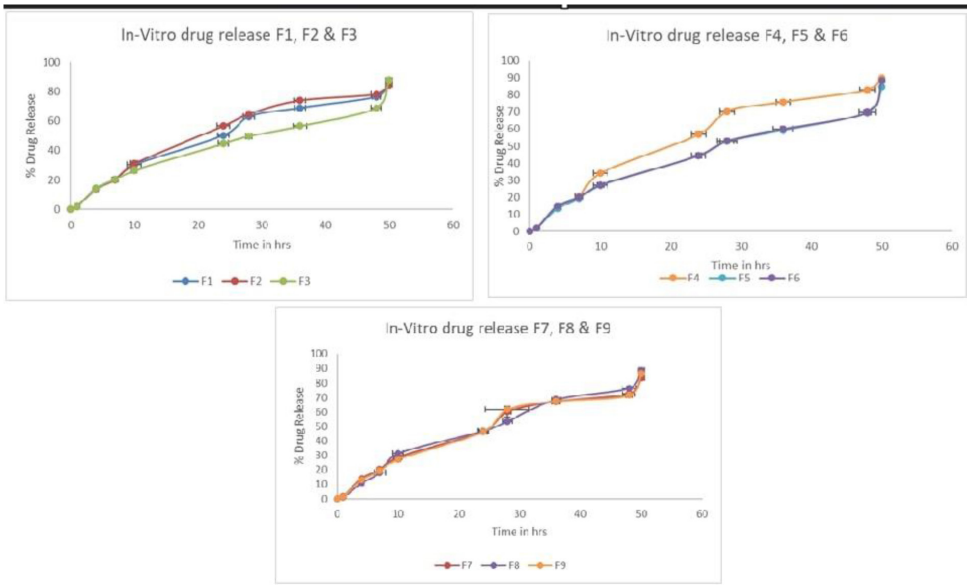


Figure 8. Graphical representation of the *in vitro* drug release profile of the formulations.

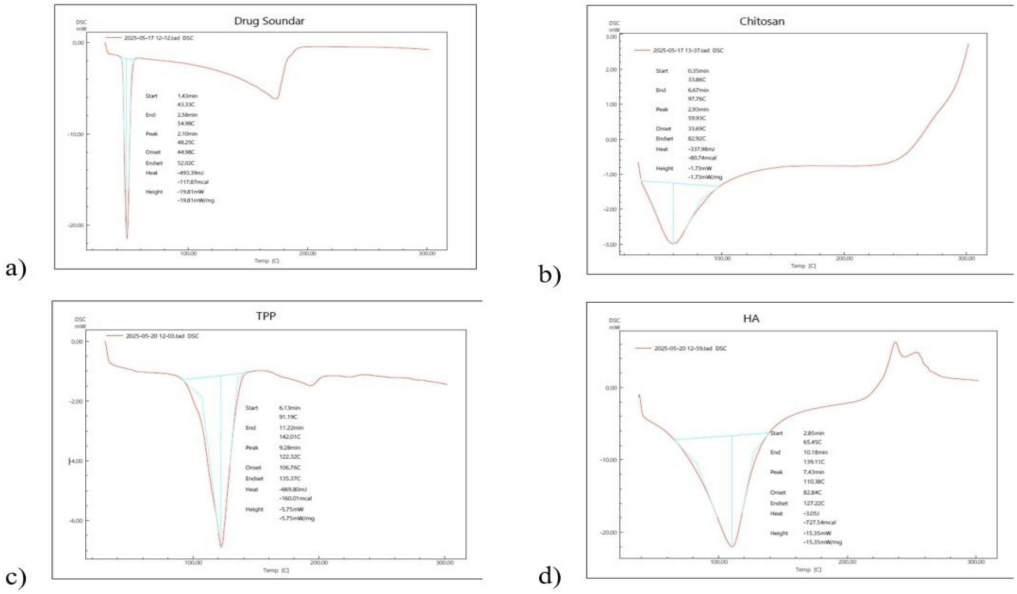


Figure 9. DSC thermographs of **(A).** Drug, **(B).** Chitosan, **(C).** TPP and **(D).** HA.

the crystalline lattice, suggesting that the drug exists in an amorphous or molecularly dispersed form within the polymer network. This transition is highly advantageous, as amorphisation enhances solubility, dissolution rate, and potential bioavailability. The findings, supported by complementary DSC data showing the absence of drug-specific melting endotherms, strongly validate successful encapsulation and compatibility within the nanoparticulate system, ensuring improved stability and therapeutic efficiency of the final formulation[63,64].

4.5.7 Drug Release Kinetics

The release data (F1–F9) were fitted to four mathematical models (zero-order, first-order, Higuchi, and Korsmeyer–Peppas) to elucidate the underlying mechanism. Among the models, the Higuchi and Korsmeyer–Peppas fits yielded the highest correlation coefficients ($R^2 > 0.98$), indicating that drug release was primarily diffusion-controlled. The zero-order and first-order models showed comparatively weaker fits, reflecting that release was not governed solely by concentration gradients or constant flux.

The Korsmeyer–Peppas exponent (n) for all formulations was in the range of 0.53–0.71, which corresponds to non-Fickian (anomalous) transport. This suggests that drug release occurred through a combined mechanism of diffusion of thymoquinone through the hydrated chitosan–HA matrix and polymer relaxation/erosion. Formulation F4, which demonstrated the highest cumulative release (~90% at 49 h), also showed the highest "n" value (~0.71), indicating a stronger contribution of matrix relaxation in sustaining drug liberation. Such biphasic release, i.e. initial burst followed by diffusion–erosion-controlled

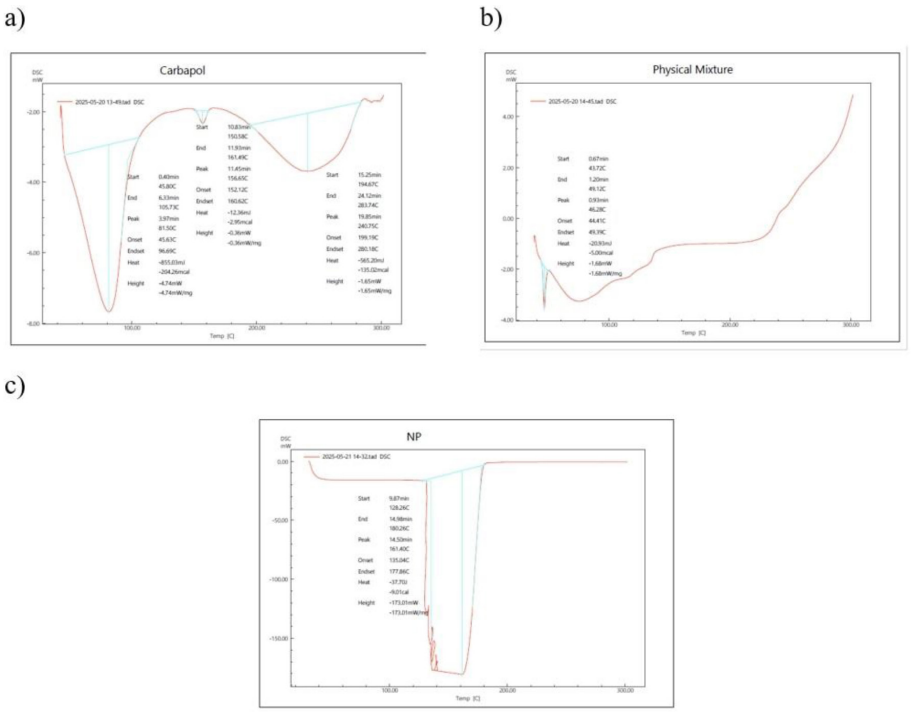


Figure 10. DSC thermographs of **(A).** Carbopol, **(B).** Physical mixture and **(C).** Nanoparticles.

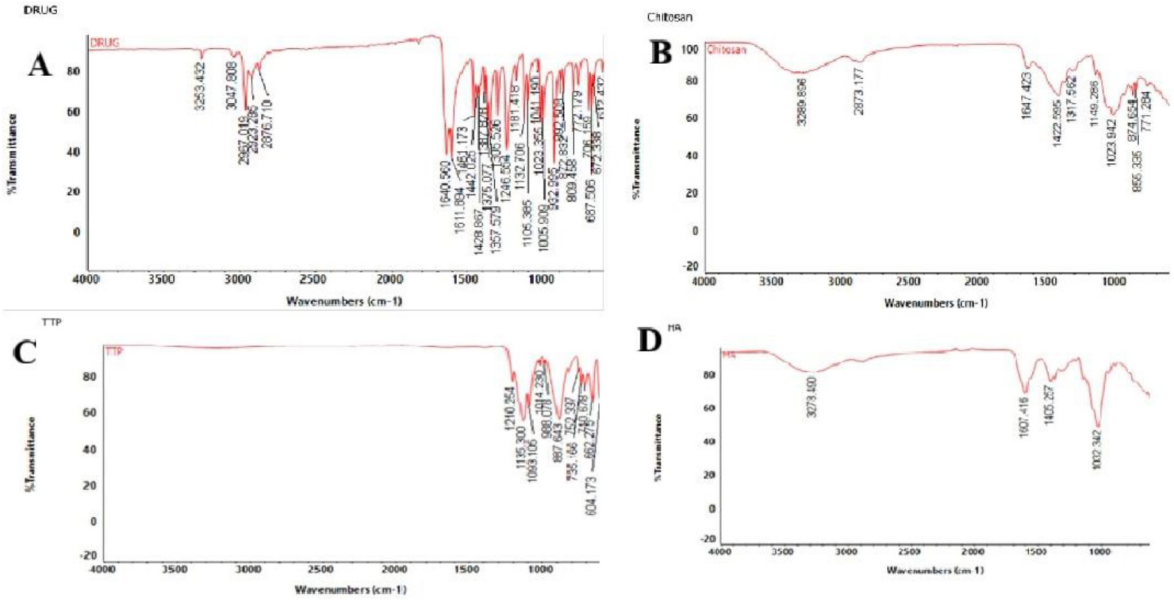


Figure 11. FTIR peaks: **(A).** Drug, **(B).** Chitosan, **(C).** TPP and **(D).** Hyaluronic acid.

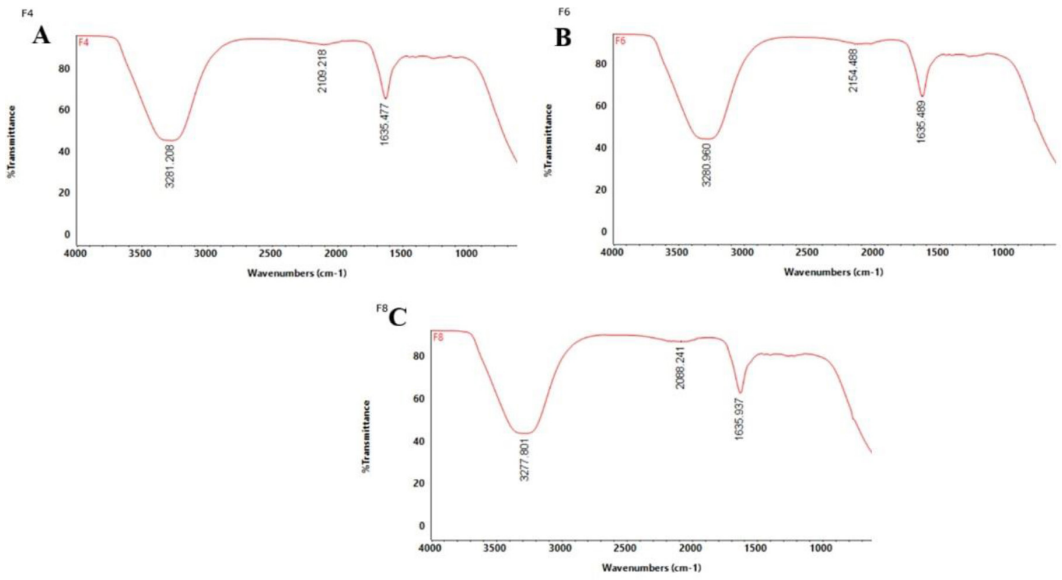


Figure 12. FTIR peaks **(A).** F4, **(B).** F6 and **(C).** F8.

release, which is a hallmark of nanoparticulate systems with polyelectrolyte coatings and has been reported in related HA–Ch nanocarriers[65,66].

These results collectively establish that the HA–Ch nanoparticles achieved a controlled release profile consistent with therapeutic requirements: an early phase ensuring immediate bioavailability followed by sustained release for prolonged activity.

4.5.8 Morphological Characterisation

Transmission Electron Microscopy (TEM) was employed to evaluate the surface morphology and structural features of the optimised nanoparticles. TEM micrographs in Figure 13 revealed well-dispersed nanosized particles with a predominantly spherical to near-spherical geometry and smooth surface architecture. The particle sizes observed by TEM (150–200 nm) were in close agreement with the dynamic light scattering (DLS) results, thereby validating the dimensional consistency of the formulations.

A distinct core–shell appearance was evident, wherein the high electron density of the chitosan–HA shell contrasted sharply with the less dense drug-loaded core. This structural delineation confirmed successful nanoparticle assembly through electrostatic complexation. The morphological uniformity observed in TEM images further supports the particle size and polydispersity index (PDI < 0.3) data, indicating the production of stable and homogenous nanosystems.

The spherical architecture of the nanoparticles is particularly advantageous for biological applications, as it promotes efficient cellular uptake via endocytosis and enhances interactions with mucosal surfaces. Similar spherical morphologies of HA–Ch nanoparticles have been reported in earlier studies, reinforcing the robustness and reproducibility of the ionic gelation approach adopted here[67].

4.5.9 Zeta Potential

The optimised nanoparticles exhibited a zeta potential of –28.7 mV, indicating the presence of a moderately high negative surface charge. Such a value suggests sufficient electrostatic repulsion among particles to prevent aggregation, which is consistent with the observed low PDI (<0.3). Generally, nanoparticles with zeta potential values beyond ±25 mV are considered to possess good colloidal stability due to the strong interparticulate repulsive forces that counteract van der Waals attractions.

The negative charge can be primarily attributed to the ionised carboxyl groups of hyaluronic acid (HA) on the nanoparticle surface, which remained dominant despite the presence of positively charged chitosan during electrostatic complexation. This finding confirms the successful coating of the nanoparticle surface with HA, leading to a negative zeta potential.

From a biological perspective, a moderately negative surface charge is advantageous. It minimises nonspecific

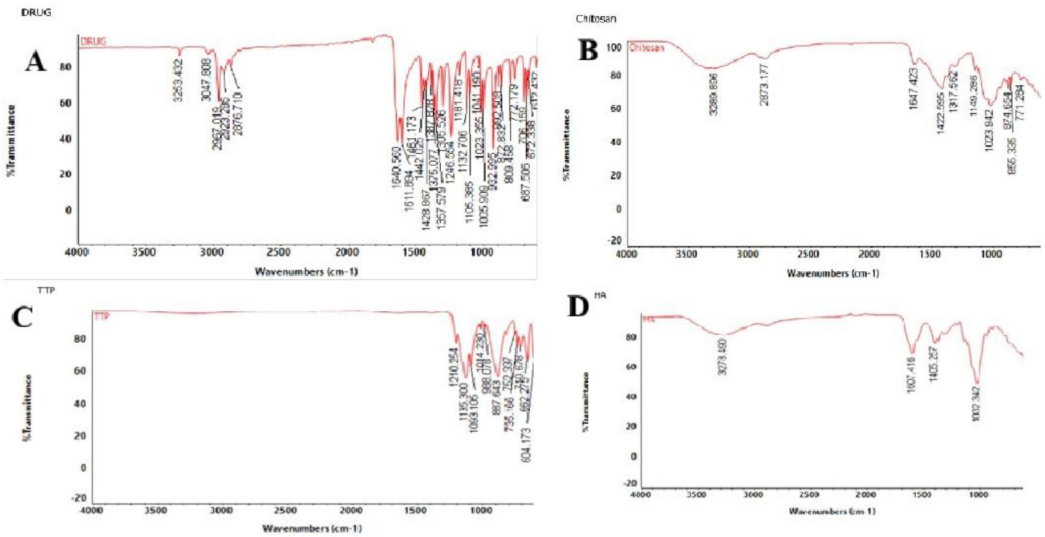


Figure 13. TEM images of nanoparticles.

protein adsorption and reduces rapid clearance by the reticuloendothelial system (RES), thereby enhancing systemic circulation time. Furthermore, the negative charge favorsmucoadhesion with positively charged sites on mucosal surfaces, improving retention at the site of administration. Comparable studies on HA–Chnanosystems have reported zeta potentials in the range of –25 to –35 mV, supporting the stability and biological applicability of the present formulation[67].

5. Conclusion

This work successfully developed and optimised hyaluronic acid–chitosan nanoparticles for thymoquinone delivery using a systematic statistical design approach. The optimised system demonstrated nanoscale size, uniform distribution, high drug entrapment, negative zeta potential, and controlled release, supported by FTIR and TEM analyses. Collectively, these features confirm effective drug encapsulation, structural stability, and compatibility of the formulation. The conversion of thymoquinone into an amorphous molecularly dispersed state further enhances its dissolution and bioavailability potential. Such attributes make the optimised nanoparticles a promising candidate for the management of rheumatoid arthritis. Future studies should focus on *in vivo* pharmacokinetic evaluation, long-term stability assessment, and therapeutic efficacy in disease models to confirm clinical applicability.

6. References

1. Aletaha D, Smolen JS. Diagnosis and management of rheumatoid arthritis: a review. Journal of the American medical association. 2018; 320(13):1360–1372. https://doi.org/10.1001/jama.2018.13103 PMid: 30285183.
2. Black RJ, Cross M, Haile LM, Culbreth GT, Steinmetz JD, Hagins H, *et al*. Global, regional, and national burden of rheumatoid arthritis, 1990–2020, and projections to 2050: a systematic analysis of the Global Burden of Disease Study 2021. Lancet Rheumatol. 2023; 5(10):e594–610. https://doi.org/10.1016/S2665-9913(23)00211-4 PMid: 37795020 PMCid: PMC10546867.
3. Smolen JS, Landewé RBM, Bijlsma JWJ, Burmester GR, Dougados M, Kerschbaumer A, *et al*. EULAR recommendations for the management of rheumatoid arthritis with synthetic and biological disease-modifying antirheumatic drugs: 2019 update. Ann Rheum Dis. 2020; 79(6):685–699. https://doi.org/10.1136/annrheumdis-2019-216655 PMid: 31969328.
4. Singh JA, Saag KG, Bridges SL Jr, Akl EA, Bannuru RR, Sullivan MC, *et al*. 2015 American College of Rheumatology guideline for the treatment of rheumatoid arthritis. Arthritis Rheumatol. 2016; 68(1):1–26. https://doi.org/10.1002/art.39480 PMid: 26545940 PMCid: PMC12473059.
5. Arjumand S, Shahzad M, Shabbir A, Yousaf MZ. Thymoquinone attenuates rheumatoid arthritis by downregulating TLR2, TLR4, *T*NF-α, IL-1, and NF-κB expression levels. Biomed Pharmacother. 2019; 111:958–963. https://doi.org/10.1016/j.biopha.2019.01.006 PMid: 30841475.
6. Vaillancourt F, Silva P, Shi Q, Fahmi H, Fernandes JC, Benderdour M. Elucidation of molecular mechanisms underlying the protective effects of thymoquinone against

rheumatoid arthritis. J Cell Biochem. 2011; 112(1):107–117. https://doi.org/10.1002/jcb.22884 PMid: 20872780.
7. Ahmad A, Husain A, Mujeeb M, Khan SA, Najmi AK, Siddique NA, *et al*. A review on therapeutic potential of *Nigella sativa*: a miracle herb. Asian Pac J Trop Biomed. 2013; 3(5):337–352. https://doi.org/10.1016/S2221-1691(13)60075-1 PMid: 23646296 PMCid: PMC3642442.
8. Darakhshan S, Bidmeshki Pour A, Hosseinzadeh Colagar A, Sisakhtnezhad S. Thymoquinone and its therapeutic potentials. Pharmacol Res. 2015; 95–96:138–158. https://doi.org/10.1016/j.phrs.2015.03.011 PMid: 25829334.
9. Pal RR, Rajpal V, Singh P, Saraf SA. Recent findings on thymoquinone and its applications as a nanocarrier for the treatment of cancer and rheumatoid arthritis. Pharmaceutics. 2021; 13(6):775. https://doi.org/10.3390/pharmaceutics13060775 PMid: 34067322 PMCid: PMC8224699.
10. Danaei M, Dehghankhold M, Ataei S, Hasanzadeh Davarani F, Javanmard R, Dokhani A, *et al.* Impact of particle size and polydispersity index on the clinical applications of lipidic nanocarrier systems. Pharmaceutics. 2018; 10(2):57. https://doi.org/10.3390/pharmaceutics10020057 PMid: 29783687 PMCid: PMC6027495.
11. Torchilin VP. Multifunctional nanocarriers. Adv Drug Deliv Rev. 2012; 64:302–315. https://doi.org/10.1016/j.addr.2012.09.031
12. Ahmed TA, Aljaeid BM. Preparation, characterization, and potential application of chitosan, chitosan derivatives, and chitosan metal nanoparticles in pharmaceutical drug delivery. Drug Des Devel Ther. 2016; 10:483–507. https://doi.org/10.2147/DDDT.S99651 PMid: 26869768 PMCid: PMC4734734.
13. Puluhulawa LE, Joni IM, Elamin KM, Mohammed AFA, Muchtaridi M, Wathoni N. Chitosan–hyaluronic acid nanoparticles for active targeting in cancer therapy. Polymers (Basel). 2022; 14(16):3410. https://doi.org/10.3390/polym14163410 PMid: 36015667 PMCid: PMC9416118.
14. Singh A, Ahmad I, Akhter S, Jain GK, Iqbal Z, Talegaonkar S, *et al*. Nanocarrier based formulation of thymoquinone improves oral delivery: stability assessment, *in vitro* and *in vivo* studies. Colloids Surf B Biointerfaces. 2013; 102:822–832. https://doi.org/10.1016/j.colsurfb.2012.08.038 PMid: 23104039.
15. Rathore C, Rathbone MJ, Chellappan DK, Tambuwala MM, Pinto TDJA, Dureja H, *et al*. Nanocarriers: more than tour de force for thymoquinone. Expert Opin Drug Deliv. 2020; 17(4):479–494. https://doi.org/10.1080/17425247.2020.1730808 PMid: 32077770.
16. Taguchi G. Introduction to quality engineering: designing quality into products and processes. Tokyo: Asian Productivity Organization; 1986.
17. Roy RK. A primer on the Taguchi method. 2nd ed. Dearborn, MI: Society of Manufacturing Engineers; 2010.
18. Ahmed TA, Aljaeid BM. Preparation, characterization and potential application of chitosan, chitosan derivatives and chitosan metal nanoparticles in pharmaceutical drug delivery. Drug Des Devel Ther. 2016; 10:483–507. https://doi.org/10.2147/DDDT.S99651 PMid: 26869768 PMCid: PMC4734734.
19. Danaei M, Dehghankhold M, Ataei S, Hasanzadeh Davarani F, Javanmard R, Dokhani A, *et al*. Impact of particle size and polydispersity index on the clinical applications of lipidic nanocarrier systems. Pharmaceutics. 2018; 10(2):57. https://doi.org/10.3390/pharmaceutics10020057 PMid: 29783687 PMCid: PMC6027495.
20. Torchilin VP. Multifunctional nanocarriers. Adv Drug Deliv Rev. 2012; 64:302–315. https://doi.org/10.1016/j.addr.2012.09.031
21. Montgomery DC. Design and analysis of experiments. 9th ed. Hoboken: Wiley; 2017.
22. Antony J. Design of experiments for engineers and scientists. 2nd ed. Oxford: Elsevier; 2014.
23. Montgomery DC. Design and analysis of experiments. 9th ed. Hoboken: Wiley; 2017.
24. Myers RH, Montgomery DC, Anderson-Cook CM. Response surface methodology: process and product optimization using designed experiments. 4th ed. Hoboken: Wiley; 2016.
25. Nayak AK, Pal D. Development of pH-sensitive tamarind seed polysaccharide-alginate composite beads for controlled diclofenac sodium delivery using response surface methodology. Int J Biol Macromol. 2011; 49(4):784–793. https://doi.org/10.1016/j.ijbiomac.2011.07.013 PMid: 21816168.
26. Singh B, Ahuja N. Response surface optimization of drug delivery system. In: Jain KK, editor. Drug Delivery Systems. Totowa: Humana Press; 2008. pp. 107–126.
27. Beg S, Sandhu PS, Batra RS, Khurana RK, Singh B. QbD-based systematic development of novel optimized solid self-nanoemulsifying drug delivery systems (SNEDDS) of lovastatin with enhanced biopharmaceutical performance. Drug Deliv. 2015; 22(6):765–784. https://doi.org/10.3109/10717544.2014.900154 PMid: 24673611.
28. Hasrawati A, Rizaldi I, Febrianti D, Mursyid AM, Bakri NA. Preparation and characterization of thymoquinone nanoparticles PEGylated as drug delivery system. Univ J Pharm Res. 2021;5(6):13-17. https://doi.org/10.22270/ujpr.v5i6.506
29. Al-Qubaisi M, Rasedee A, Flaifel MH, Ahmad SH, Hussein-Al-Ali S, Hussein MZ, *et al*. Thymoquinone-loaded lipid nanocarriers: preparation, characterization and *in vitro* evaluation. Drug Des Devel Ther. 2015; 9:6335–6349. https://doi.org/10.2147/DDDT.S93239

30. Al-Qubaisi M, Rozman NAS, Abdul Rahim RA, Ahmad SH, Zainal Z. *In vitro* release and cytotoxicity of thymoquinone loaded mesoporous silica nanoparticles. Saudi Pharm J. 2022; 30(4): 523–531. https://doi.org/10.1016/j.jsps.2022.02.004 PMid: 35527827 PMCid: PMC9068565.
31. Surekha R, Sumathi T. An efficient encapsulation of thymoquinone using solid lipid nanoparticle for brain targeted drug delivery: physicochemical characterization, pharmacokinetics and bio-distribution studies. Int J Pharm Clin Res. 2016; 8(12):1616–1624.
32. Malvern Panalytical. Zetasizer Nano S90/ZS90 dynamic light scattering minimum size specification. Technical Note. Malvern, UK: Malvern Instruments; 2010.
33. Oueslati R, Khouja M, Dhouibi I, Zammel N, Guesmi A, Dhouib S, *et al*. Experimental and theoretical FTIR spectra of thymoquinone: DFT and vibrational analysis. Spectrosc Lett. 2025; 58(2):75–85. https://doi.org/10.1080/00387010.2025.2478939
34. Yıldırım M, Özcan I, Erdoğan S, Karatas A, Çalış S. Thymoquinone-loaded PHEMA-based magnetic nanoparticles: physicochemical characterization and *in vitro* anticancer evaluation. BiochimBiophys Acta Gen Subj. 2024; 1868(2):130545. https://doi.org/10.1016/j.bbagen.2024.130545.
35. Calvo P, Remuñán-López C, Vila-Jato JL, Alonso MJ. Novel hydrophilic chitosan–polyethylene oxide nanoparticles as protein carriers. J Appl Polym Sci. 1997; 63(1):125–132. https://doi.org/10.1002/(SICI)1097-4628(19970103)63:1<125::AID-APP13>3.0.CO;2-4
36. Grenha A, Seijo B, Remuñán-López C. Microencapsulated chitosan nanoparticles for lung protein delivery. Eur J Pharm Sci. 2005; 25(4–5):427–437. https://doi.org/10.1016/j.ejps.2005.04.009 PMid: 15893461.
37. Xu Y, Du Y. Effect of molecular structure of chitosan on protein delivery properties of chitosan nanoparticles. Int J Pharm. 2003; 250(1):215–226. https://doi.org/10.1016/S0378-5173(02)00548-3 PMid: 12480287.
38. Gan Q, Wang T. Chitosan nanoparticle as protein delivery carrier—systematic examination of fabrication conditions for efficient loading and release. Colloids Surf B Biointerfaces. 2007; 59(1):24–34. https://doi.org/10.1016/j.colsurfb.2007.04.009 PMid: 17555948.
39. Grenha A, Gomes ME, Rodrigues M, Santo VE, Mano JF, Neves NM, *et al*. Development of new chitosan–HA-based nanoparticles for drug delivery: synthesis and characterization. Carbohydr Polym. 2010; 79(3):633–640.
40. Mao HQ, Roy K, Troung-Le VL, Janes KA, Lin KY, Wang Y, *et al*. Chitosan–DNA nanoparticles as gene carriers: synthesis, characterization, and transfection efficiency. J Control Release. 2001; 70(3):399–421. https://doi.org/10.1016/S0168-3659(00)00361-8 PMid: 11182210.
41. Bernkop-Schnürch A, Dünnhaupt S. Chitosan-based drug delivery systems. Eur J Pharm Biopharm. 2012; 81(3):463–469. https://doi.org/10.1016/j.ejpb.2012.04.007 PMid: 22561955.
42. Montgomery DC. Design and analysis of experiments. 8th ed. Hoboken (NJ): Wiley; 2013.
43. Taguchi G, Chowdhury S, Wu Y. Taguchi's quality engineering handbook. Hoboken (NJ): Wiley-Interscience; 2005. https://doi.org/10.1002/9780470258354
44. Hu B, Pan C, Sun Y, Hou Z, Ye H, Hu B, *et al*. Optimization of fabrication parameters to produce chitosan–tripolyphosphate nanoparticles for delivery of tea catechins. J Agric Food Chem. 2008; 56(16):7451-7458. https://doi.org/10.1021/jf801111c PMid: 18627163.
45. Bernkop-Schnürch A, Dünnhaupt S. Chitosan-based drug delivery systems. Eur J Pharm Biopharm. 2012; 81(3):463-469. https://doi.org/10.1016/j.ejpb.2012.04.007 PMid: 22561955.
46. Nafee N, Schneider M, Schaefer UF, Lehr CM. Chitosan nanoparticles as drug delivery systems: a review. Int J Pharm. 2007; 332(1-2):1-22.
47. Hu B, Pan C, Sun Y, Hou Z, Ye H, Hu B, *et al*. Optimization of fabrication parameters to produce chitosan–tripolyphosphate nanoparticles for delivery of tea catechins. J Agric Food Chem. 2008; 56(16):7451-7458. https://doi.org/10.1021/jf801111c PMid: 18627163.
48. Bernkop-Schnürch A, Dünnhaupt S. Chitosan-based drug delivery systems. Eur J Pharm Biopharm. 2012; 81(3):463-469. https://doi.org/10.1016/j.ejpb.2012.04.007 PMid: 22561955.
49. Calvo P, Remuñán-López C, Vila-Jato JL, Alonso MJ. Novel hydrophilic chitosan–polyethylene oxide nanoparticles as protein carriers. J Appl Polym Sci. 1997; 63(1):125-132. https://doi.org/10.1002/(SICI)1097-4628(19970103)63:1<125::AID-APP13>3.0.CO;2-4
50. Gan Q, Wang T. Co-delivery of paclitaxel and siRNA by novel amphiphilic chitosan-based nanoparticles for synergistic cancer therapy. Biomaterials. 2007; 28(9):1387-1396.
51. Saranya N, Moorthi A, Saravanan S, Devi MP, Selvamurugan N. Chitosan and its derivatives for gene delivery. Int J Biol Macromol. 2011; 48(2):234-238. https://doi.org/10.1016/j.ijbiomac.2010.11.013 PMid: 21134396.
52. Mao HQ, Roy K, Troung-Le VL, Janes KA, Lin KY, Wang Y, *et al*. Chitosan–DNA nanoparticles as gene carriers: synthesis, characterization and transfection efficiency. J Control Release. 2001; 70(3):399-421. https://doi.org/10.1016/S0168-3659(00)00361-8 PMid: 11182210.
53. Li Z, Wu J, Wang Y, Zhuo R, Xu Y. Nanoparticles based on chitosan hydrochloride/polyaspartic acid polyelectrolyte complexes for protein delivery. Int J Pharm. 2010; 393(1-2):266-273.
54. Xu Y, Du Y. Effect of molecular structure of chitosan on protein delivery properties of chitosan nanoparticles. Int J Pharm. 2003; 250(1):215-226. https://doi.org/10.1016/S0378-5173(02)00548-3 PMid: 12480287.

55. Mao S, Shuai X, Unger F, Simon M, Bi D, Kissel T. The depolymerization of chitosan: Effects on physicochemical and biological properties. Int J Pharm. 2004; 281(1-2):45–54. https://doi.org/10.1016/j.ijpharm.2004.05.019 PMid: 15288342.
56. Almalik A, Day PJ, Tirelli N. HA-coated chitosan nanoparticles for CD44-mediated nucleic acid delivery. Int J Pharm. 2013; 458(1):181–191. https://doi.org/10.1002/mabi.201300302 PMid: 24106105.
57. Bernkop-Schnürch A, Dünnhaupt S. Chitosan-based drug delivery systems. Eur J Pharm Biopharm. 2012; 81(3):463–469. https://doi.org/10.1016/j.ejpb.2012.04.007 PMid: 22561955.
58. Sonaje K, Lin KJ, Wey SP, Lin CK, Yeh TH, Nguyen HN, *et al*. Biodistribution, pharmacodynamics and pharmacokinetics of insulin analogues in chitosan nanoparticles following oral administration. Biomaterials. 2010; 31(12):3384–3394. https://doi.org/10.1016/j.biomaterials.2010.01.042 PMid: 20149435.
59. Li J, Mooney DJ. Designing hydrogels for controlled drug delivery. Nat Rev Mater. 2016; 1(12):16071. https://doi.org/10.1038/natrevmats.2016.71 PMid: 29657852 PMCid: PMC5898614.
60. Zhang N, Wardwell PR, Bader RA. Polysaccharide-based micelles for drug delivery. Pharmaceutics. 2013; 5(2):329–352. https://doi.org/10.3390/pharmaceutics5020329 PMid: 24300453 PMCid: PMC3834947.
61. Vivek K, Sahoo SK. Encapsulation of hydrophobic drugs in polymer nanoparticles: strategies, challenges and solutions. Nanomedicine. 2011; 6(4):485–502.
62. Saremi S, Atyabi F, Dinarvand R. Chitosan-based nanoparticles for drug delivery: advances in design and applications. Curr Pharm Des. 2015; 21(29):4269–4289.
63. Coates J. Interpretation of infrared spectra, a practical approach. In: Meyers RA, editor. Encyclopedia of Analytical Chemistry. Wiley; 2000. pp. 10815–10837. https://doi.org/10.1002/9780470027318.a5606
64. Stuart B. Infrared spectroscopy: fundamentals and applications. John Wiley and Sons; 2004. https://doi.org/10.1002/0470011149
65. Dash S, Murthy PN, Nath L, Chowdhury P. Kinetic modeling on drug release from controlled drug delivery systems. Acta Pol Pharm. 2010; 67(3):217–223.
66. Siepmann J, Siepmann F. Mathematical modeling of drug delivery. Int J Pharm. 2008; 364(2):328–343. https://doi.org/10.1016/j.ijpharm.2008.09.026
67. Kalam MA. Development of chitosan nanoparticles coated with hyaluronic acid for topical ocular delivery of dexamethasone. Int J Biol Macromol. 2016; 89:127-136. https://doi.org/10.1016/j.ijbiomac.2016.04.070 PMid: 27126165.

Author Contribution

Ravimanne: Conceptualised the research study, designed the methodology, carried out the literature survey, and prepared the initial draft of the manuscript; Madhavi Patel and Mohan Maruga Raja: Served as the research guides; provided continuous guidance throughout the study, offered critical insights during data interpretation and manuscript development, and reviewed and refined the content for clarity, accuracy, and scientific rigour and also, contributed to shaping the overall structure of the study, provided constructive feedback during manuscript preparation, and assisted with final revisions to improve the quality of the manuscript. All authors have read and agreed to the published version of the manuscript.